Metall. Res. Technol. **123**, 319 (2026)
© EDP Sciences, 2026
https://doi.org/10.1051/metal/2026020

&Metallurgical Research Technology

Available online at:
www.metallurgical-research.org

Original Article

Characterization of molybdenum-modified aluminide coating on 304 stainless steel via slurry aluminizing

Ibrahim Owolabi Ambali[1,2], Tan Siew Min[1], Anasyida Abu Seman[1,*], Tuti Katrina Abdullah[1], Khairunisak Abdul Razak[1], Brij Kumar Dhindaw[3], and Yusuf L. Shuaib-Babata[2]

[1] School of Materials and Minerals Resources Engineering, Engineering Campus, Universiti Sains Malaysia, 14300 Nibong Tebal, Penang, Malaysia
[2] University of Ilorin, Faculty of Engineering and Technology, Ilorin, Nigeria
[3] Indian Institute of Technology Kharagpur 721302, India

Received: 6 January 2026 / Accepted: 19 January 2026

Abstract. This study investigates the microstructural changes and growth kinetics of intermetallic compounds in Mo-modified aluminide coatings on 304 stainless steels with varying temperatures and times. Molybdenum and alumina were introduced via slurry aluminizing. Heat treatments were conducted at 750 °C, 800 °C, and 850 °C for varying times (6, 8, and 10 h). Aluminide coating was characterized with SEM, EDX, and XRD, revealed the presence of multilayer phases comprising of Fe-Al and Mo-Al intermetallic compounds, along with an alumina scale on the coating surface. Samples heated at 750 °C showed uniform coatings, while those at 800 °C and 850 °C exhibited voids and cracks. The growth kinetics of the coating obey a parabolic law conforming to diffusion-controlled growth. The activation energies calculated for FeAl and Fe_3Al were 360 kJ/mol and 237 kJ/mol, respectively, which is higher than that of coatings containing aluminium (FeAl layer: 180 kJ/mol and and Fe_3Al layer: 260 kJ/mol). The total activation energy (Q) was 26 kJ/mol for coatings containing molybdenum and 53 kJ/mol for coatings with only aluminium. Hardness of the intermetallic layers varied from 378 to 966 HV for Mo-modified coatings as compared to aluminide coating (380 to 1030 Hv). The corrosion behaviour of Mo-aluminide coatings was investigated in 3.5% NaCl using polarization and electrochemical impedance spectroscopy (EIS) tests. Results show improved performance of corrosion resistance due to Mo-rich intermetallic phases, with the 6 h sample exhibiting the best corrosion resistance.

Keywords: slurry aluminizing / molybdenum / SS304 / Fe-Al intermetallic compound / Mo-Al intermetallic compound / growth kinetics / corrosion

1 Introduction

Aluminide coating and alumina film form on the surface of materials (low carbon, iron-based alloys, steel, or Ni-based alloys) offer significant promise in mitigating corrosion of materials for high-temperature applications [1]. The Fe-Al intermetallic layer compound formed on the surface of the sample can serve as the active layer necessary for the self-repair of the aluminium oxide film. There are several methods of forming aluminide coating. Still, slurry has been a stand-out technique and the most interesting due to its ease of manufacturing, environmental friendliness, and cost-effectiveness [2]. Slurry aluminizing techniques are considered an intermediary condition between chemical vapour deposition and the hot dip process, containing aluminium as the metal source, and are applied to the substrate and heat-treated to form Fe-Al intermetallic compounds. During the aluminizing process, atoms diffuse either inward or outward to form aluminide layers, depending on the coating parameters. The typical intermetallic compounds form on Fe-based alloy are Fe_2Al_5, Fe_3Al, and FeAl [3].

Fe-Al intermetallic compounds were attractive for structural applications due to adequate strength and low density at temperatures below 600ty 6 °C. However, ductility dropped at 25 °C, and a sharp decrease in strength was observed beyond 600ty 6 °C. The limited strength of Fe-Al intermetallic compounds has also been identified as a challenge for their use in high-temperature applications. The limited strength might be attributed to the brittle nature of intermetallic compounds (IMCs)-Fe_2Al_5. Thus, the alloying element was added to enhance room-temperature ductility and high-temperature strength.

* e-mail: anasyida@usm.my

The alloying element added could form precipitation hardening, solid solution strengthening, binary intermetallic compounds, and ternary intermetallic compounds [4]. Molybdenum (Mo) plays a key role in improving the performance of Fe-Al intermetallic compounds. Adding Mo to the aluminide coating is believed to inhibit the outward diffusion of aluminium by occupying the vacancy sites in the Fe_2Al_5 crystal structure, thus enhancing the coating's mechanical stability in a harsh environment [5,6].

Baligidad [7] mentioned that the addition of Mo in Fe_3Al enhances both yield strength and creep rupture at 600 °C, due to solid solution strengthening and precipitation strengthening mechanisms. Hitech et al. [8] investigated the dilution of molybdenum on aluminium surface and observed that the formation of Al-Mo phases (Al_5Mo and Al_8Mo_3) could enhance corrosion resistance for high-temperature applications. Recent studies have shown that molybdenum significantly influences the microstructure, where even small changes in coating composition can modify phase formation and morphological characteristics [9].

Understanding the Fe-Al-Mo phase diagram is crucial for designing Fe-Al intermetallic compound formation, as it offers insights into the phases present at operational temperatures, along with their compositions and volume fractions [10]. The effects of inward and outward growth on the microstructure and characteristics of Mo-modified aluminide coatings remain inadequately explored. This study evaluates the influence of molybdenum additions on the microstructure and growth kinetics of intermetallic layers formed on 304 stainless steel, along with hardness. Although aluminide coatings are primarily developed for high-temperature oxidation/hot-corrosion protection, room-temperature electrochemical testing in 3.5% NaCl was additionally used here as a rapid screening method to evaluate the corrosion resistance of modified slurry aluminizing at various temperatures and times.

2 Material and methods

The substrate used is austenitic stainless steel, 304 SS grade with dimensions of 10 mm × 10 mm × 2 mm. The samples were ground manually under the flow of water and ultrasonically cleaned in acetone; thereafter, rinsed with distilled water, and finally dried using a hot air dryer. The composition and slurry preparation adopted have been mentioned somewhere [11]. In this study, the slurry composition used is (70% Al, 15% Al_2O_3, and 15% Mo).

The slurry was applied on the substrate using a Sagola spray gun. A total mass-to-area ratio of 20–30 mg/cm^2 was achieved by carefully controlling the coating process. The aluminizing treatment was conducted at temperatures of 750 °C, 800 °C, and 850 °C for 6, 8, and 10 h in a Carbolite furnace under an argon atmosphere at the controlled heating rate of 10 °C per minute, then furnace cooling to room temperature. Heat-treated samples were then embedded in epoxy resin, ground by silicon carbide paper from grade 240–2000 and polished to a mirror-like finish with alumina paste from 1 μm down to 0.05 μm. The samples were etched for 3–5 s using the standard Keller's reagent in accordance with ASTM E407-07 [12].

The microstructure of the aluminized layer in the cross-section was characterized using FESEM (ZEISS SUPRA 35VP) coupled with Energy Dispersive X-ray Spectrometer (EDX). The phase identification in the aluminized samples was evaluated using X-ray diffraction (XRD), Bruker Advanced D8 with Cu Kα radiation (λ = 0.15406 nm), 2θ scanning from 10° to 90°. The coating thickness was measured using FESEM, and the microhardness was performed on the coating under the load of 25 g for 15s using a Vickers microhardness tester (LECO microindentation hardness tester LM248AT). The Arrhenius equation was adopted to estimate the activation energy of the intermetallic layers as follows.

$$X^2 = Kt, \tag{1}$$

$$K = K_0 \exp\left(\frac{-Q}{RT}\right), \tag{2}$$

$$\ln K = (\ln K_0) - Q/RT. \tag{3}$$

X means coating thickness (μm), K means growth rate constant (μm/s), and t means aluminizing time of slurry (s).

K_o means pre-exponential constant, Q means activation energy (J), T means absolute temperature (K), and R is the gas constant 8.314J/(k.mol) [13].

The electrochemical corrosion test measurements were performed using the AUTOLAB model PGSTAT 302N Potentiostat/galvanostat with a standard three-electrode cell containing a reference electrode, a counter electrode, and a working electrode (coating samples) at ambient temperature (25 °C). Electrochemical impedance spectroscopy (EIS) was employed to investigate the corrosion behaviour of the coating samples. A Metrohm Auto lab electrochemical analyzer loaded with Nova software was used to analyze the data from the test. Potentiodynamic polarization curves, or Tafel polarization curves scanning ranged from −0.20 V to +0.20 V, with a scanning rate of 10 mV for the corrosion potential (E*corr*) as shown in Figure 1. The EIS measurement was carried out with frequency ranges, from 100 kHz to 10 mHz together with an amplitude sinusoidal wave of 10 mV and an OCP of 300s waiting time.

3 Results

3.1 SEM/EDX analysis of aluminide coating

Figure 2 presents the SEM image of aluminized samples heat-treated at 750 °C, 800 °C, and 850 °C for 6 and 10 h. The formation mechanism of intermetallic compound resulting from interdiffusion between the substrate and the coating (Al, Mo, and Al_2O_3) with Al and Mo as the main diffusing species into the substrate, while Fe diffuses outwards the substrate, resulting in the formation of intermetallic compounds formed at different layers as shown in Figure 3. The addition of filler Al_2O_3 favours the formation of Fe-rich intermetallic compounds [14,15].

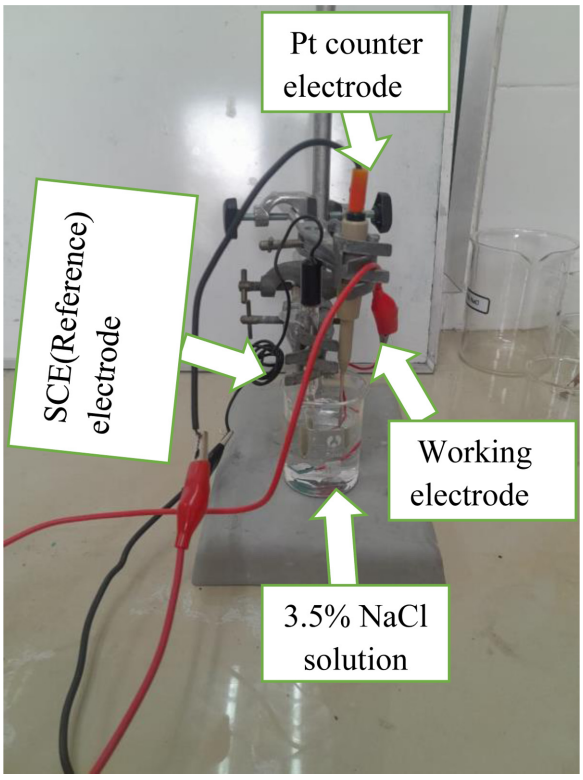

Fig. 1. Linear polarization and EIS setup of the experiment.

Cross-sectional morphology of the sample heat-treated at 750 °C and 800 °C reveals that the images are continuous, uniform, and comprise three distinct layer structures (Layer 1, 2, and 3), which can be categorized as outer layer, middle layer, and inner layer. However, for the sample heat-treated at 850 °C, the aluminide layer became discontinuous and transformed into a two-layer structure (Layer 1 and 2). Voids were presented under all conditions, but their size increased with higher temperatures and longer soaking times. They became prominent at 800 °C and 850 °C across all soaking durations. Overall, both the void density and size increases with increasing temperature and time, likely due to non-equilibrium elemental diffusion driven by interdiffusion and vacancy flux (known as the Kirkendall effect) [1,16]. Sun et al. [17] also reported the presence of FeAl and Fe_3Al phases accompanied by significant void formation after prolonged heat treatment (30 h). The formation of a void can compromise the mechanical properties of the coating and diminish its effectiveness as protective barrier. The Kirkendall effect serves as a diffusion pathway for potentially harmful substances, posing risks of degradation and delamination of the coating [18].

The EDX spectra for the samples heat-treated at 750 °C and 800 °C exhibit similar elemental distributions, as shown in Figure 4. Aluminium and iron are the primary diffusing element with the identified intermetallic compounds are consistent with those predicted by the Al-Fe binary phase diagram. To confirm this, EDX spot analysis was conducted on the sample heat-treated at 750 °C, 800 °C and 850 °C for 6 h as tabulated in Table 1. At 750 °C, Spot 1 showed 27.69 at.% Fe and 61.89 at.% Al, while spot 2 exhibited 19.13 at.% Fe and 51.16 at.% Al, corresponding to Fe_2Al_5. Fe_2Al_5 and $FeAl_3$ are Al-rich, brittle intermetallic compounds typically observed on the outer coating surface. Spot 3 indicated the presence of FeAl with 40.66 at.% Fe and 41.36 at.% Al, whereas spot 4 showed 65.81 at.% Fe and 5.87 at.% Al, characteristic of Fe_3Al. These Fe-rich intermetallics are located near the substrate. Overall, Fe_2Al_5, FeAl, and Fe_3Al were identified as the dominant phases in samples heat-treated at 750 °C and 800 °C.

At 850 °C, spot analysis of Layer 1 reveals a composition of 41.62 at.% Fe and 39.61 at.% Al at Spot 1, corresponding to the FeAl phase. In contrast, another region exhibits 60.27 at.% Fe and 11.07 at.% Al, consistent with the Fe_3Al phase. These intermetallics are identified as the dominant phases across all heat treatment durations of 6, 8, and 10 h at 850 °C. Both FeAl and Fe_3Al are known for their inherent toughness and ductility [3]. In the present study, the presence of Fe_2Al_5, $FeAl_3$, FeAl, and Fe_3Al is consistent with previous findings [3,17]. Although Al–Mo phases (also referred to as Mo–Al phases) are difficult to identify by EDX due to the low molybdenum content, their presence can be inferred from the interdiffusion process. Due to the limited Mo level, Mo–Al intermetallics are expected to form as fine precipitates, predominantly within the outer/additive region.

3.2 Phase analysis

Figure 5 depicts XRD analysis to validate the presence of intermetallic phases as specified by the SEM/EDX. Four phases of the Fe-Al intermetallic compound according to the Fe-Al binary system were identified. The dominant phases detected are FeAl (ICDD PDF number: 04-013-9779) and Fe_3Al (ICDD PDF number: 04-013-9781) for all the samples heat-treated at different temperatures and soaking times. Fe_2Al_5 (ICDD PDF number: 00-029-0043) and $FeAl_3$ (ICDD PDF number 00-069-0296) were detected at 750 °C for 6 h, as shown in Figure 5a. Similar observations have been previously reported [3,19,20]. Fe_2Al_5 and $FeAl_3$ progressively transform into more ductile phases, namely FeAl (ICDD PDF No. 04-013-9779) and Fe_3Al (ICDD PDF No. 04-013-9781) and was formed at 750 °C for 8 and 10 h. The same phases formed and detected by XRD for the sample heat-treated at 800 °C for 6, 8, and 10 h, as illustrated in Figures 5a and 5b.

Figure 5c shows the phases detected by the XRD for the sample heat-treated at 850 °C for 6, 8, and 10 h where Fe_2Al_5 and $FeAl_3$ have fully transformed into the denser and more ductile FeAl and Fe_3Al phases, which dominate the microstructure throughout. A similar transformation was reported by Sun et al. [17], where Fe_2Al_5 and $FeAl_3$ completely disappeared after 30 h of heat treatment at 700 °C, resulting in a uniform aluminide coating composed of FeAl and Fe_3Al, with no internal cracking observed. XRD also detected the alumina phase, Al_2O_3 (ICDD PDF number: 01-088-4954), that formed as a result of unreacted Al with oxygen [21].

Apart from the dominant Fe-Al phases, XRD also identified Mo-Al intermetallic phases in the samples heat-treated at 750 °C, 800 °C, and 850 °C across all soaking durations. The $MoAl_5$ phase (ICDD PDF No. 00-029-0050)

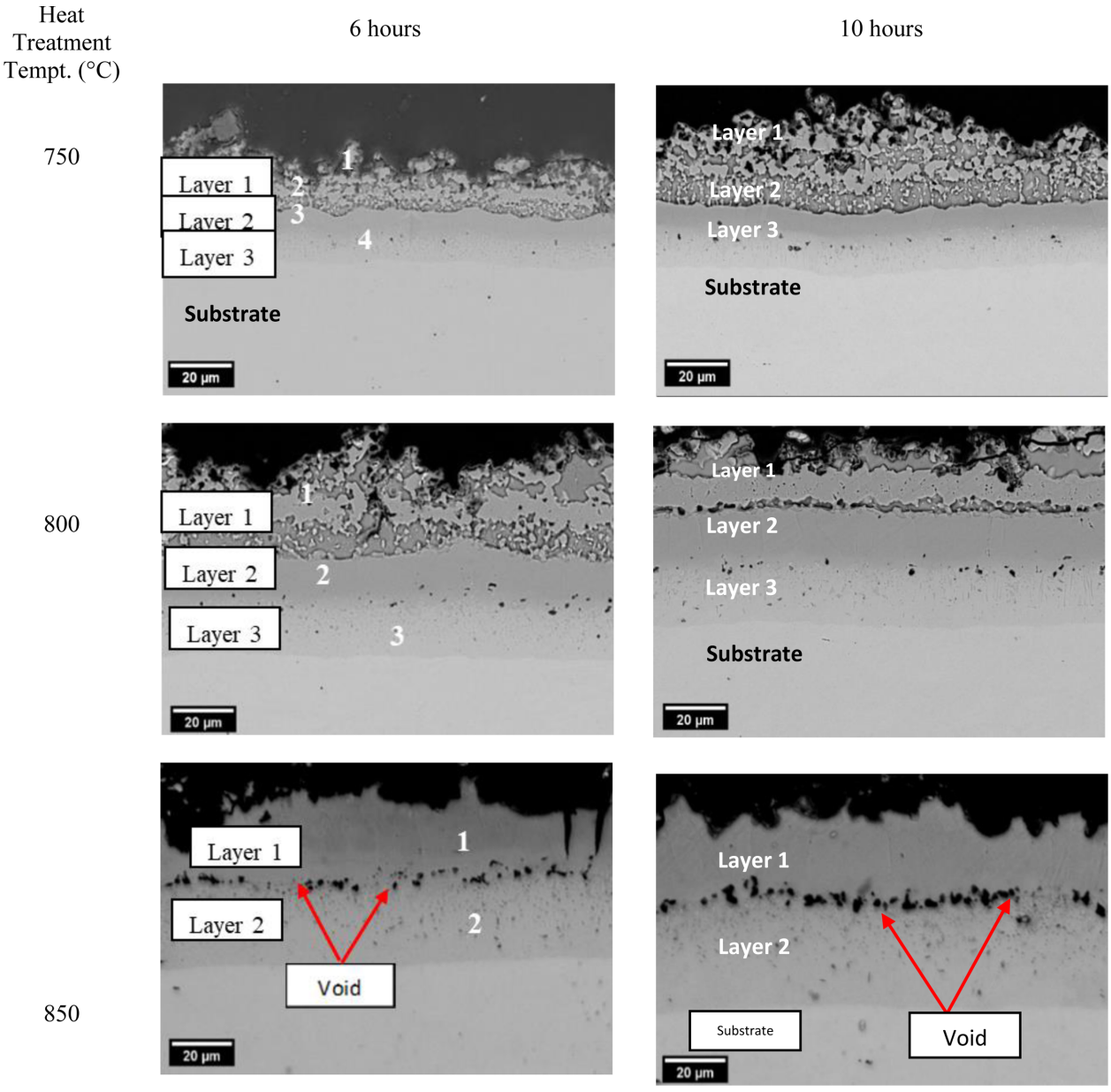

Fig. 2. Cross-section image of Mo-aluminide coating samples heat-treated at 750, 800, and 850 °C for 6 and 10 h.

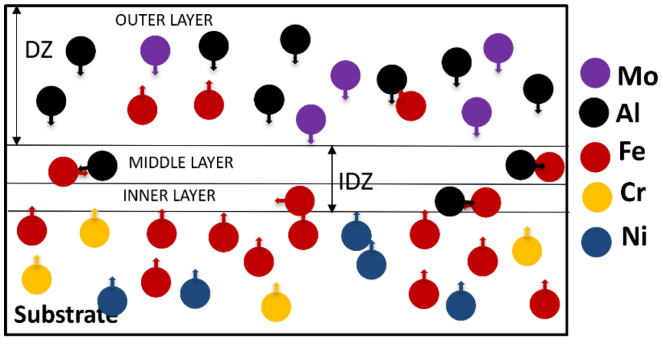

Fig. 3. Schematic diagram of interdiffusion between coating and substrate.

was consistently detected at all conditions and aligns with earlier findings reported by [22]. At 750 °C for 6 and 8 h, Mo_3Al_8 (ICDD PDF No. 00-029-0050) was observed, indicating the formation of Al-rich intermetallics in the Mo-Al system, in agreement with [23,24] findings. Upon increasing the soaking time to 10 h, Mo_3Al_8 was observed to transform into $MoAl_4$ (ICDD PDF No. 04-004-2308), stable up to 850 °C for 6 h. This is consistent with the transformations reported by Ponweiser et al. [25]. At 850 °C for 8 and 10 h, $MoAl_4$ disappeared, allowing transformation for the formation of ductile FeAl and Fe_3Al phases. These findings underscore the importance of precise temperature control during the aluminizing process, as it directly influences phase evolution and

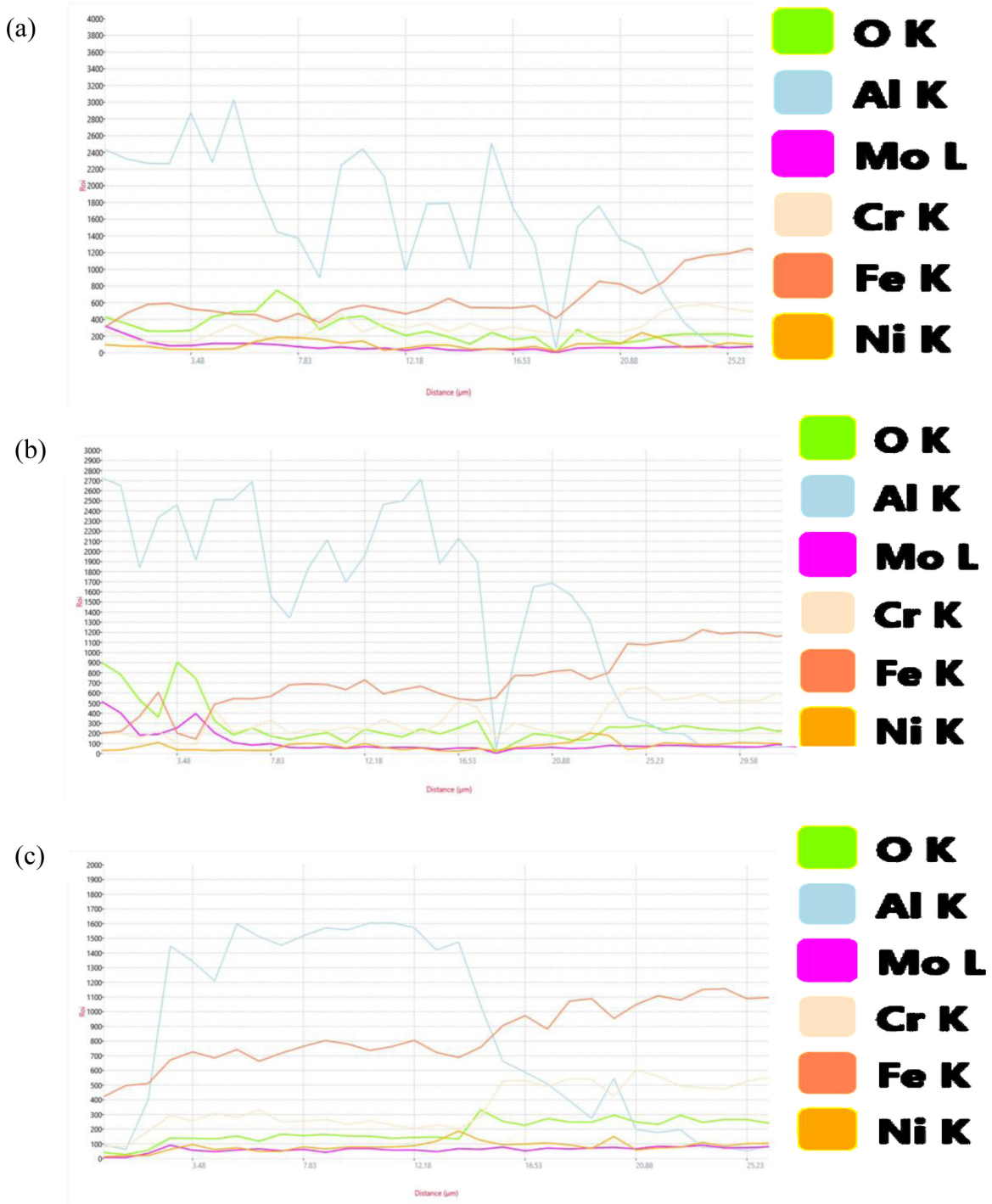

Fig. 4. X-Ray elemental profiles of the Mo-modified aluminide coating for the samples heat-treated at (a) 750 °C, (b) 800 °C, and (c) 850 °C for 6 h.

coating efficiency. Lower temperatures may lead to incomplete transformation and reduced efficiency, whereas higher temperatures may enhance ductility but can also introduce porosity. The presence of pores is due to the unequal interdiffusion rates (also known as the Kirkendall effect) between the coating and the substrate elements during the aluminizing process, which is more pronounced at higher temperatures. The reactions of formation of intermetallic compounds for both Fe-Al and Al-Mo intermetallics during the aluminizing process are depicted in equations (4)–(9).

Al-Mo Intermetallic formation:

$$3Mo + 8Al(l) \rightarrow Al_8Mo_3, \tag{4}$$

Table 1. EDX chemical composition on spots 1, 2, 3, 4 aluminide layer for sample heat treated at 750 °C, 800 °C, and 850 °C for 6 h.

Aluminizing temperature	Time	EDX Spot	Element (at.%)					
			Fe	Al	Cr	Ni	O	Mo
750 °C	6 h	1	27.69	61.89	3.09	2.04	4.49	0.81
		2	19.13	51.16	17.07	2.54	9.2	0.89
		3	40.66	41.36	7.51	7.51	2.2	0.75
		4	65.81	5.87	22.81	2.08	2.54	0.90
800 °C	6 h	1	22.12	57.39	14.57	0.86	3.05	2.01
		2	38.34	44.57	7.3	5.31	3.79	0.69
		3	55.63	16.64	20.49	4.78	1.71	0.76
850 °C	6 h	1	41.62	39.61	8.05	6.04	3.79	0.89
		2	34.47	44.36	7.14	4.11	9.24	0.68
		3	60.27	11.07	20.88	3.37	3.47	0.94

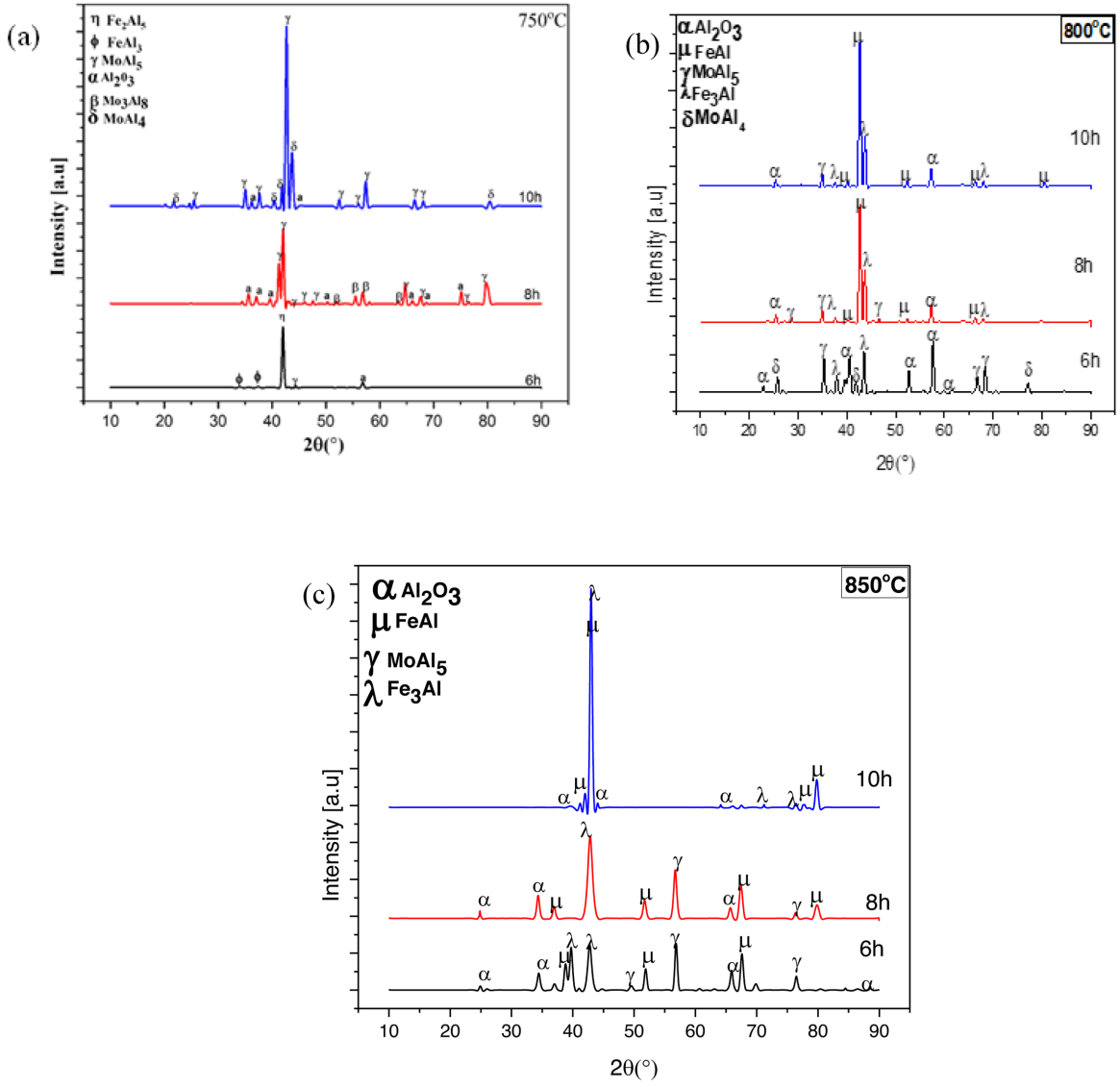

Fig. 5. XRD pattern of the Mo-modified aluminide coating heat treated at (a) 750 °C, (b) 800 °C, and (c) 850 °C for 6 h, 8 h, and 10 h.

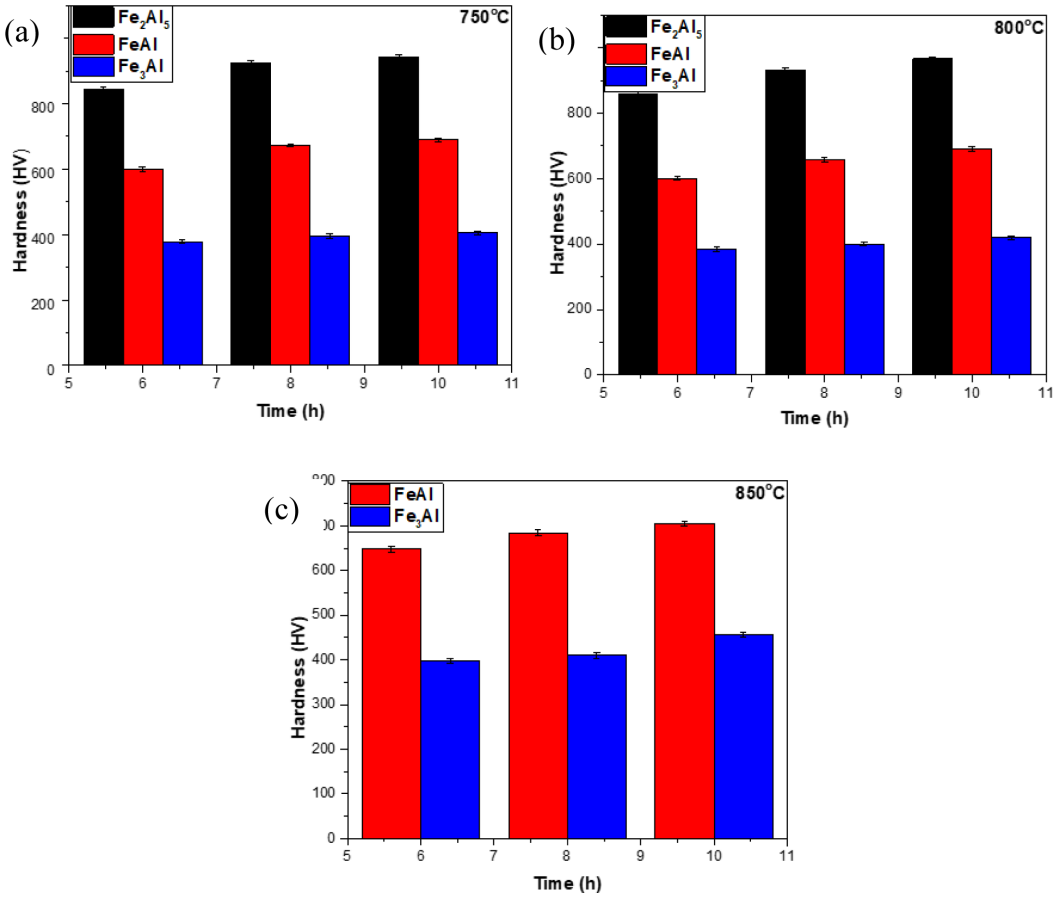

Fig. 6. Vickers hardness value of cross-section for samples heat treated at (a) 750 °C, (b) 800 °C, and (c) 850 °C for 6, 8, and 10 h.

$$Al_8Mo_3 + 4Al(l) \rightarrow 3Al_4Mo. \quad (5)$$

These phases have been identified as $Al_g(Fe, Mo)_3$, $Al_4(Fe, Mo)$ as ascribed by Du et al 2009 [26]

Fe-Al Intermetallic formation

$$2Fe + 5[Al] \rightarrow Fe_2Al_5, \quad (6)$$

$$Fe_2Al_5 + [Al] \rightarrow 2FeAl_3, \quad (7)$$

$$Fe_2Al_5 + 3Fe \rightarrow 5FeAl, \quad (8)$$

$$3Fe + [Al] \rightarrow Fe_3Al. \quad (9)$$

3.3 Microhardness

Figure 6 presents the hardness measurements of the intermetallic compounds (Fe_2Al_5, FeAl, and Fe_3Al) in heat-treated samples at 750 °C, 800 °C, and 850 °C for durations of 6, 8, and 10 h. The high hardness values were attributed to the aluminium concentration in the coating layer, identified as the Al-rich zone. In this study, the maximum hardness of 966.4 HV was recorded at 800 °C for 10 h. However, as temperature and time increased, the hardness of the intermetallic compound (IMC) decreased due to the transition in the IMC. Previous studies have shown that increased aluminizing temperature and soaking time generally led to higher hardness values [27]. Fe_2Al_5 was not found for the sample heat-treated at 850 °C for all the soaking times. This may be is attributed to the addition of molybdenum, which influenced interdiffusion and the reduction of Fe_2Al_5, given room for more ductile phases (FeAl and Fe_3Al).

Fe_2Al_5 consistently exhibited the highest hardness values across all heat-treated conditions, ranging from 840 to 970 HV. The reported hardness values of Fe_2Al_5 from literature were between 820 to 1030 HV without the addition of molybdenum [19]. A decrease in hardness value was observed due to the transition from the additive layer to the interdiffusion zone (IDZ), which produced an Fe-rich zone, due to the high concentration of Fe at the substrate. The average hardness values for the FeAl and Fe_3Al layers dropped and were approximately recorded between (599.6–705.3) HV and (378.6–457.2) HV, respectively. The reported hardness range for the FeAl phase is between 580 and 710 HV, while for Fe_3Al, it is between 380 and 470 HV for aluminium coating without addition of molybdenum [27,28]. The substrate exhibited a hardness value of 219.1 HV. The addition of Mo slowing the interdiffusion and stabilizing inner layer (typically FeAl/Fe_3Al) which is less brittle than Fe_2Al_5. Thus the addition of Mo slightly reduced the hardness of coating.

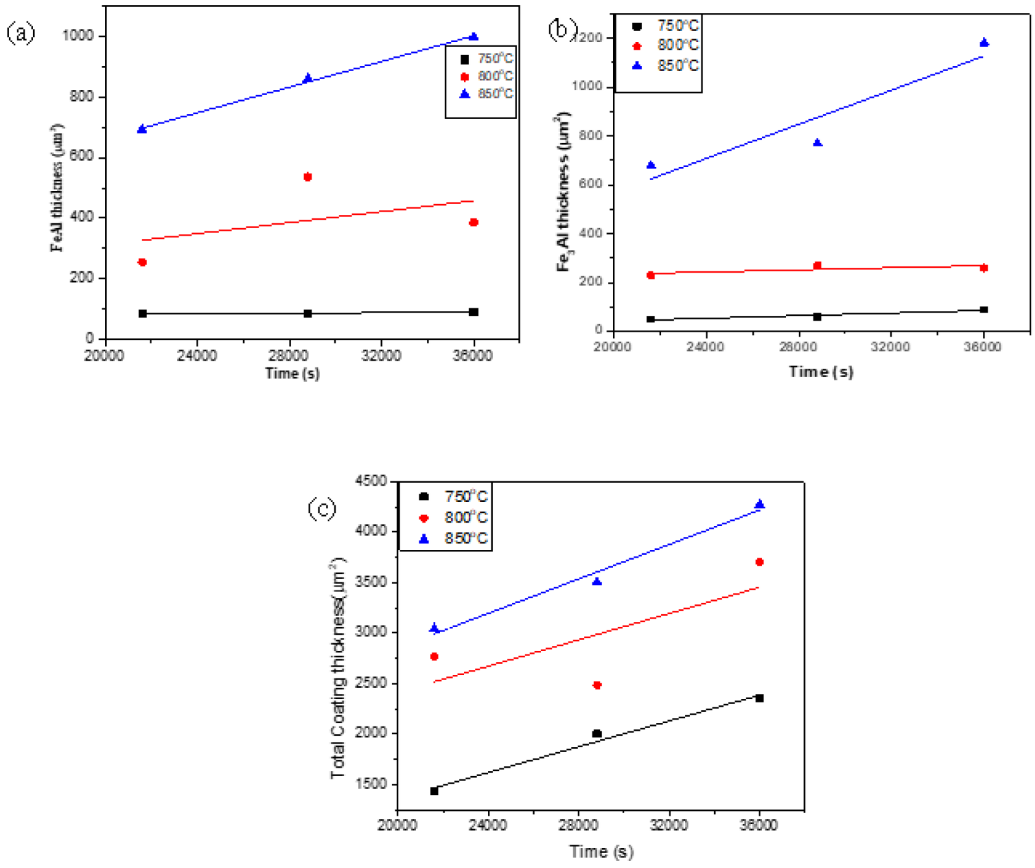

Fig. 7. Plot of the square of coating thickness (μm) vs time (s)for (a) FeAl, (b) Fe_3Al (c) Total IML coating.

3.4 Growth kinetics of aluminide coating

The growth of intermetallic compounds is diffusion-controlled and has been proposed by [29,30] Interdiffusion between the Fe and Al determined the coating thickness layers during the slurry aluminizing. Figure 7 presents the square of the coating thickness for FeAl and Fe_3Al layers as a linear relationship with the time (s) from equation (1), which determines the growth rate constant (K) values. Arhenius's equation indicates the parabolic relation between the thickness of the aluminide layers and time at various aluminizing temperatures. The slope of plotted lines in Figure 8 determines the activation energy of aluminide layers (FeAl, Fe_3Al, and overall coating).

The value of activation energy obtained for FeAl was 360 kJ/mol, while for Fe_3Al, it was 237 kJ/mol. The value is much higher as reported for aluminide coating without molybdenum (FeAl layer : 180 kJ/mol and and Fe_3Al layer : 260 kJ/mol) [29]. The overall activation energy in this work was determined as 26 kJ/mol, which is lower than the activation energy for coating containing aluminium only (53 kJ/mol). Activation energy values reported in the literature [27] are typically categorized as follows: (i) below 100 kJ/mol, (ii) between 100–200 kJ/mol, and (iii) between 200–300 kJ/mol for coating containing aluminium only. The higher activation energy values observed for FeAl and Fe_3Al in this study can be attributed to the influence of molybdenum (Mo) on the aluminide coating. Mo contributes to the diffusion control of Al and Fe, promoting the growth of ductile phases. The addition of molybdenum has been reported to significantly influence phase evolution within Fe–Al-based intermetallic systems. Mo acts as a diffusion-affecting element that alters the thermodynamic stability and growth behavior of ordered FeAl and Fe_3Al [31,32]. Conversely, the lower overall activation energy is linked to the reduced coating thickness, as Mo occupies vacancy sites in the Fe_2Al_5 crystal structure, facilitating the formation of more FeAl and Fe_3Al phases.

3.5 Corrosion behaviour

3.5.1 Corrosion behaviour by linear polarisation

Figure 9 illustrates the Tafel polarization curve for samples heat-treated at 750 °C for 6, 8, and 10 h. Linear fitting parameters [(b_a), (b_c), *Ecorr, Icorr*, *R*p, and CR] values are displayed in Table 2. The higher corrosion resistance of the coating is associated with a more positive corrosion potential and a smaller passivation current density. Sample heat-treated at 750 °C for 6 h exhibited the lowest corrosion rate, indicating the superior corrosion resistance, with a measured value of 3.18×10^{-3} mm/yr while the sample heat-treated at 750 °C for 10 h has the highest corrosion rate. It has been reported that the higher the polarization resistance, the better the corrosion resistance [21]. The lower the I*corr*, the better the corrosion, and the higher the E*corr*, the better the corrosion resistance [33,34]. The decline in corrosion was suggested due to the void found in the coating.

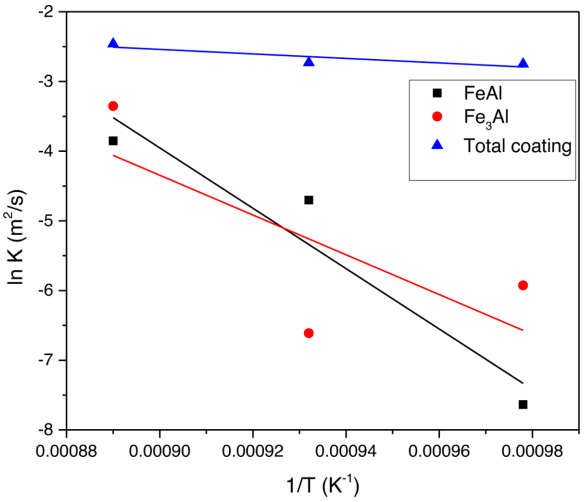

Fig. 8. Plot of ln K Vs 1/T for FeAl , Fe_3Al, and Total IML.

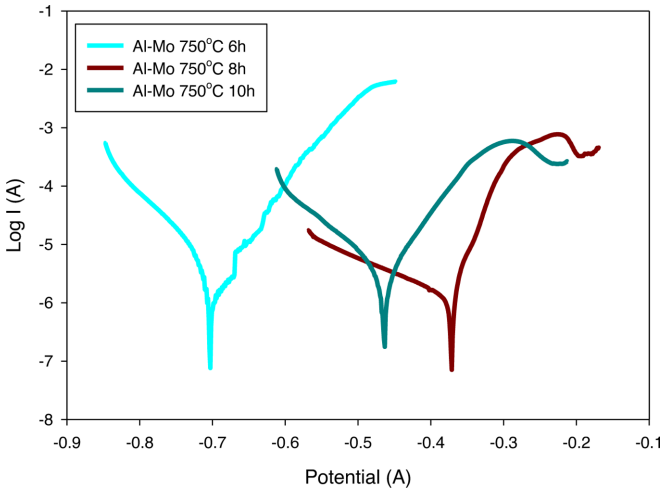

Fig. 9. Tafel polarization curves for Mo-modified aluminide coating heat-treated for 750 °C at 6, 8, and 10 h.

Table 2. Electrochemical parameters obtained from the polarisation curves.

Samples	Electrochemical corrosion measurements					
	Anodic slope (b_a)	Cathodic slope (b_c)	*E*corr (V)	*R*p (Ω cm^2)	*I*corr (μA cm^{-2})	CR (mm/year)
750 °C 6 h	0.024	0.021	−0.649	15686	3.098×10^{-1}	3.18×10^{-3}
750 °C 8 h	0.044	0.016	−0.373	10249	5.117×10^{-1}	5.252×10^{-3}
750 °C 10 h	0.135	0.085	−0.464	4266	5.293	5.434×10^{-2}

The improved corrosion resistance was observed at lower aluminizing temperatures and shorter diffusion times due to the differences in layer thickness ratio, phase distribution, and defect density, even though Mo–Al phases form under all conditions. At lower temperatures and shorter durations, diffusion rates of Al, Fe, and Mo are significantly reduced, leading to the formation of thinner, more compact, and compositionally uniform layers. This controlled diffusion minimizes the formation of brittle Fe_2Al_5-type intermetallics and reduces the likelihood of Kirkendall porosity. The outer layer becomes enriched with stable Al-rich and Mo-Al phases (MoAl), which provide a high Al chemical activity needed for continuous and dense Al_2O_3 scale formation during corrosion.

3.5.2 Electrochemical impedance spectroscopy (EIS)

Electrochemical impedance spectroscopy (EIS) was employed to enable a more detailed assessment of the corrosion behaviour of the coatings and to validate the findings obtained from linear polarization tests. A quantitative comparison between the Nyquist plots and polarization data indicates that both techniques revealed consistent corrosion trends across the samples. The larger the capacitive loop diameter in Nyquist, the better the corrosion resistance, the larger the impedance in the Bode modulus, the larger the phase angle, the better the corrosion resistance. This theory has been established in the literatures [35–37]. Figure 10a depicts the Nyquist curve for the sample heat-treated at 750 °C for 6, 8, and 10 h for the Mo-modified aluminide coating. The semicircle loop diameter for the sample heat-treated at 750 °C for 6 h exhibited the largest loop among the tested samples, indicating the best corrosion resistance.

The sample heat-treated for 6 h demonstrated a broader phase angle range centred around the maximum angle, with a wider frequency span, indicating enhanced corrosion resistance relative to the 6 and 8 h samples, as shown in Figures 10b and 10c for the Bode phase and Bode modulus.

According to the equivalent circuit model as tabulated in Table 3, Rs denotes the solution resistance, while Rp and CPE correspond to the coating's polarization resistance and constant-phase element, respectively. The use of a constant-phase element in place of an ideal capacitor is justified by the surface heterogeneity and diffusion phenomena, as reported by [37]. The fitted EIS parameters derived from the Nyquist as mentioned above, Bode modulus, and Bode phase plots are summarized in Table 3, for each heat treatment condition: (a) 750 °C for 6 h, (b) 750 °C for 8 h, and (c) 750 °C for 10 h. Notably, the sample heat-treated at 750 °C for 6 h exhibited the highest polarization resistance value (Rp) of 348 Ω·cm^2 with the lowest value CPE 46.58×10^{-6}, indicating superior corrosion resistance when compared to the samples treated for 8 and 10 h. The results are consistent with the previous

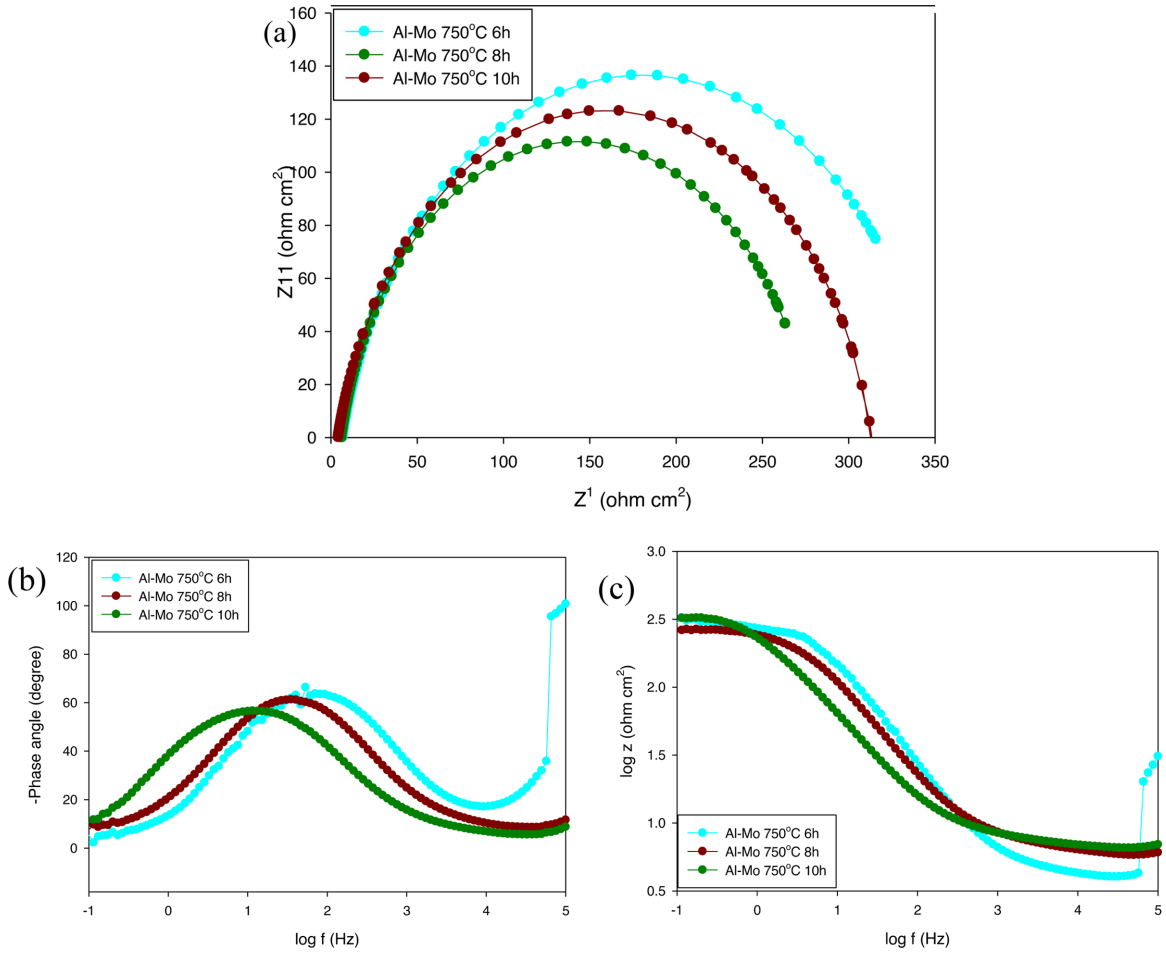

Fig. 10. (a) Nyquist, (b) Bode, and (c) Bode phase plots for the sample heat-treated for 750 °C at 6, 8, and 10 h.

Table 3. Values for different elements of the electric equivalent circuits obtained for Mo-modified aluminide coating heat-treated for 750 °C at 6, 8, and 10 h.

			CPE	
Samples	R_s (Ω cm^{-2})	R_P (Ω cm^{-2})	$Y_0 \times 10^{-6}$ μS s^n cm^{-2}	n
750 °C 6 h	4.18	348	46.58	0.998
750 °C 8 h	6.16	274	166	0.998
750 °C 10 h	6.64	309	452	0.997

studies [36]. In additon, the linear potentiodynamic polarization test result is consistent with the electrochemical impedance spectroscopy.

4 Conclusion

Mo-modified aluminide coatings applied via slurry techniques were successfully developed on 304SS substrates. Several conclusions were derived from the studies.

– The aluminide coating developed on the substrate consists of multiple Fe-Al intermetallic phases, including Fe_2Al_5, $FeAl_3$, Fe_3Al, and FeAl, with newly developed intermetallic layers at the interface, including Mo_3Al_8, $MoAl_4$, and $MoAl_5$. These phases form in order because of thermally activated diffusion of Al, Fe, and Mo.
– The incorporation of Mo and Al_2O_3 lowers the chemical activity of Al within the coating, which promotes the development of more ductile Fe-Al intermetallic. This modification results in a smoother and more coherent coating/substrate interface. With increasing temperature, accelerated diffusion promotes preferential growth of the FeAl and Fe_3Al layers, although greater porosity and void formation were also observed.

- The growth of the FeAl and Fe_3Al phases in the Mo-modified aluminide system follows thermally activated diffusion, with calculated activation energies of 360 kJ/mol for FeAl and 237 kJ/mol for Fe_3Al, confirming their kinetic behaviour and stability at high temperature.
- Coating hardness increases with higher temperature and longer exposure time as Fe–Al intermetallic layers continuously form and thicken. The peak hardness is observed in the Al-rich Fe_2Al_5 region of the sample treated at 850 °C for 10 h, confirming Fe_2Al_5 as the hardest phaseThe sample heat-treated at 750 °C for 6 h demonstrates the highest corrosion resistance, attributed to the balanced formation of protective intermetallic phases and a more stable microstructure with fewer voids compared to higher-temperature treatments.
- The sample heat-treated at 750 °C for 6 h exhibits the highest corrosion resistance, likely due to an optimal balance of protective intermetallic phases and a more stable microstructure with fewer voids than those produced at higher temperatures.

Acknowledgments

The author gratefully acknowledged the School of Materials and Mineral Resources Engineering, Universiti Sains Malaysia for facilities and as well as sponsorship by TETFund, Nigeria (TETF/ES/UNIV/KWARA/TSAS/2021).

Funding

This research received internal funding from USM Bridging Grant: R501-LR-RND003-0000002181-0000.

Conflicts of interest

The authors declare that they have no known competing financial interests or personal relationships that could have appeared to influence the work reported in this paper.

Data availability statement

Data will be made available on request.

Author contribution statement

A.O. Ibrahim: Writing – original draft, Methodology, Investigation. **S.M. Tan:** Investigation. **A.S. Anasyida:** Writing – review & editing, conceptualization, Supervision, Project administration, Funding acquisition. **T.K. Abdullah:** Conceptualization, Supervision. **K.A. Razak, B.K. Dhindaw & Y. Shuaib-Babata:** Conceptualization.

References

1. T.N. Prasanthi, C. Sudha, P.S. Reddy, Hot dip aluminization of 304L SS and P91 ferritic-martensitic steel – Comparison of interface morphology and growth kinetics of reaction zones, Surf. Coatings Technol. **440**, 128465 (2022)
2. M. Masoumi Balashadehi, P. Nourpour, A. Sabour Rouh Aghdam et al., The formation, microstructure and hot corrosion behaviour of slurry aluminide coating modified by Ni/Ni-Co electrodeposited layer on Ni-base superalloy, Surf. Coatings Technol. **402**, 126283 (2020)
3. J. Dong, Y. Sun, F. He, Formation mechanism of multilayer aluminide coating on 316L stainless steel by low-temperature pack cementation, Surf. Coatings Technol. **375**, 833–838 (2019)
4. S.C. Deevi, Advanced intermetallic iron aluminide coatings for high temperature applications, Prog. Mater. Sci. **118**, 100769 (2021)
5. M. Kotkowiak, A. Piasecki, M. Kotkowiak et al., Heat-resisting aluminized coatings modified by chromium addition produced on nickel-based alloys, Trans. Indian Inst. Met. **71**, 2919–2931 (2018)
6. M.C. Galetz, B. Rammer, M. Schütze, The protection of aluminides by alloying with molybdenum in high chlorine containing atmospheres at 1,000 C, Oxid. Met. **81**, 151–165 (2014)
7. R.G. Baligidad, A. Radhakrishna, A. Datta et al., Effect of molybdenum addition on structure and properties of high carbon Fe3Al based intermetallic alloy, Mater. Sci. Eng. A **313**, 117–122 (2001)
8. H.D. Vora, R.S. Rajamure, S. Soundarapandian et al., Dilution of molybdenum on aluminum during laser surface alloying, J. Alloys Compd. **570**, 133–143 (2013)
9. E. Kocaman, Effect of the molybdenum content on wear and corrosion behavior of Fe-B-based surface-alloyed layer, Coatings **13**, (2023). https://doi.org/10.3390/coatings13122050
10. Z. Du, C. Guo, C. Li et al., Thermodynamic description of the Al-Mo and Al-Fe-Mo systems, J. Phase Equilibria Diffus. **30**, 487–501 (2009)
11. I.O. Ambali, A.A. Seman, T.K. Abdullah, Microstructural evolution and hardness properties of Si-modified aluminide coating on 304 stainless steel via slurry aluminizing: effect of aluminizing temperatures, **20**, 152–161 (2024)
12. S. Practice, Standard practice for microetching metals and alloys, ASTM E-407, **07**, 1–22 (2016)
13. O. Ambali, S.M. Tan, M.A. Jalaluddin et al., Investigation of Al 2 O 3 -modified aluminide on 304SS : microstructural evolution, Hardness and Growth Kinetic through Slurry Aluminizing, **72**, 1–12 (2024)
14. M.K. Javan, A. Azizi Moghaddam, M. Farvizi et al., Effect of aluminum to alumina particles size ratio on the microstructural aspects of aluminide coatings by LTHA pack cementation, Mater. Res. Express **6**, 096437 (2019)
15. T. Kepa, F. Pedraza, F. Rouillard, Intermetallic formation of Al-Fe and Al-Ni phases by ultrafast slurry aluminization (flash aluminizing), Surf. Coatings Technol. **397**, (2020). https://doi.org/10.1016/j.surfcoat.2020.126011
16. C. Zhang, H. Feng, Z. Zheng et al., Preparation and corrosion behavior of the Al-modified MoSi2/Al2O3 coating on the surface of molybdenum metal core, Corros. Sci. **193**, 109879 (2021)
17. Y. Sun, J. Dong, P. Zhao et al., Formation and phase transformation of aluminide coating prepared by low-temperature aluminizing process, Surf. Coatings Technol. **330**, 234–240 (2017)

18. P. Audigié, V. Encinas-Sánchez, S. Rodríguez et al., High temperature corrosion beneath carbonate melts of aluminide coatings for CSP application, Sol. Energy Mater. Sol. Cells **210**, (2020). https://doi.org/10.1016/j.solmat.2020.110514
19. R.M. Triani, L.F.D.A. Gomes, R.J.T. Aureliano et al., Production of aluminide layers on AISI 304 stainless steel at low temperatures using the slurry process, J. Mater. Eng. Perform. **29**, 3568–3574 (2020)
20. T. Yener, A. Erdogan, M.S. Gök et al., Formation, characterization, and wear behavior of aluminide coating on mirrax® ESR steel by low-temperature aluminizing process, J. Tribol. **143**, (2021). https://doi.org/10.1115/1.4047667
21. B. Karpe, K. Prijatelj, M. Bizjak et al., Corrosion properties of aluminized 16Mo3 Steel, J. Min. Metall. Sect. B Metall. **59**, 91–100 (2023)
22. T. Yener, Low temperature aluminising of Fe-Cr-Ni super alloy by pack cementation, Vacuum **162**, 114–120 (2019)
23. Z. Yang, J. tao Lu, P. Zhang et al., Oxidation performance and degradation mechanism of the slurry aluminide coating deposited on Super304H in steam at 600–650 °C, Surf. Coatings Technol. **391**, 125700 (2020)
24. A.E. Kochmanska, A. Jarlaczynska, J. Baranowska, Formation of silicide and silicide-aluminide coatings on molybdenum alloy during slurry cementation process: influence of slurry volume, Materials (Basel). **14**, (2021). https://doi.org/10.3390/ma14226940
25. N. Ponweiser, W. Paschinger, A. Ritscher et al., Phase equilibria in the Al-Mo-Si system, Intermetallics **19**, 409–418 (2011)
26. T. Fu, Y. Zhang, Z. Han et al., Morphology, phase composition, surface roughness evolution and growth mechanism of hot-dip aluminum coating on Mo substrate, J. Mater. Res. Technol. **28**, 1405–1414 (2024)
27. F. Zarei, H. Nuranian, K. Shirvani, Characterization, growth kinetics and high-temperature oxidation behavior of aluminide coating formed on HH309 stainless steel by casting and subsequent heat treatment, Intermetallics **120**, 106742 (2020)
28. A.T.K. Ambali Ibrahim Owolabi, A.A. Seman, Low-temperature slurry aluminizing : investigating the influence of aluminizing time on the corrosion performance of aluminide coating on 304 SS low-temperature slurry aluminizing : investigating the influence of aluminizing time on the corrosion performa, (2024). https://doi.org/10.1088/1742-6596/2907/1/012003
29. S. Kobayashi, T. Yakou, Control of intermetallic compound layers at interface between steel and aluminum by diffusion-treatment, Mater. Sci. Eng. A **338**, 44–53 (2002)
30. Y. Yang, F. Zhang, J. He et al., Microstructure, growth kinetics and mechanical properties of interface layer for roll bonded aluminum-steel clad sheet annealed under argon gas protection, Vacuum **151**, 189–196 (2018)
31. C. Liu, T.K.S. Kumar, Ordered intermetallic alloys, Part I : Nickel andIron Aluminides, (1993)
32. S. Wiesner, L. Gerdt, K. Bobzin et al., Effect of alloying elements on growth behavior of intermetallic compounds at the cold-sprayed coating / steel interface during immersion in aluminum melt, **12**, 712–721 (2018)
33. Y.J. Hwang, Y. Kim, S.H. Park et al., Wear and corrosion properties of pure Mo coating layer manufactured by atmospheric plasma spray process, Arch. Metall. Mater. **69**, 81–85 (2024)
34. X. Zhao, J. Liu, Q. Yin et al., Preparation and properties of Al/Si coating with excellent formability and corrosion resistance on steel plate, Mater. Today Commun. **36**, 106525 (2023)
35. X. Liu, J. Xiong, Y. Lv et al., Study on corrosion electrochemical behavior of several different coating systems by EIS, Prog. Org. Coatings **64**, 497–503 (2009)
36. I. Mohammadi, A. Afshar, S. Ahmadi, Al2O3/Si3N4 nanocomposite coating on aluminum alloy by the anodizing route: Fabrication, characterization, mechanical properties and electrochemical behavior, Ceram. Int. **42**, 12105–12114 (2016)
37. J.R. Xavier, S.P. Vinodhini, Multifunctional nanocomposite coating for aluminium alloy: Corrosion resistance, flame retardancy, and mechanical enhancement for automotive components, Mater. Chem. Phys. **323**, 129628 (2024)

Cite this article as: Ibrahim Owolabi Ambali, Tan Siew Min, Anasyida Abu Seman, Tuti Katrina Abdullah, Khairunisak Abdul Razak, Brij Kumar Dhindaw, Yusuf L. Shuaib-Babata, Characterization of molybdenum-modified aluminide coating on 304 stainless steel via slurry aluminizing, Metall. Res. Technol. 123, 319 (2026) https://doi.org/10.1051/metal/2026020